Molecular interactions in N-[(2-hydroxyl)-propyl-3-trimethyl ammonium] chitosan chloride-sodium alginate polyelectrolyte complexes

Yang, Xiaodeng; Wang, Beibei; Qiao, Congde; Li, Zhi; Li, Yan; Xu, Chunlin; Li, Tianduo

Published in:
Food Hydrocolloids

DOI:
10.1016/j.foodhyd.2019.105400

Published: 01/03/2020

Document Version
Accepted author manuscript

Molecular interactions in N-[(2-hydroxyl)-propyl-3-trimethyl ammonium] chitosan chloride-sodium alginate polyelectrolyte complexes

Xiaodeng Yang[a,*], Beibei Wang[a], Congde Qiao[a], Zhi Li[a], Yan Li[a,*], Chunlin Xu[b], Tianduo Li[a]

[a] Shandong Provincial Key Laboratory of Molecular Engineering, Qilu University of Technology-Shandong Academy of Science, Ji'nan 250353, PR China.

[b] Process Chemistry Centre, Laboratory of Wood and Paper Chemistry, Åbo Akademi University, Turku, FI-20500 Finland.

* Corresponding Author: Xiaodeng Yang, E-mail: yangxiaodeng@qlu.edu.cn;
Yan Li, Email: liyan2554666@163.com;
Tel.: +86-531-89631208.

List of the subdivisions

HTCC: *N*-[(2-Hydroxyl)-propyl-3-trimethyl ammonium] chitosan chloride

DS: degree of substitution

FTIR: Fourier transform infrared spectroscopy

SEM: scanning electron microscopy

DSC: differential scanning calorimetry

DMA: dynamic-mechanical analysis

$m_{\mathrm{HTCC}}/m_{\mathrm{SA}}$: mass ratio of HTCC to SA

PEC: polyelectrolyte complex

SA: sodium alginate

EPTAC: 2,3-epoxypropyltrimethyl ammonium chloride

$-N(CH_3)_3^+$: N,N,N-trimethylammonium group

$-COO^-$: carboxyl group

ATR: attenuated total reflectance

T_g: glass-transition temperature

LJ: Lennard-Jones

SPC: simple point charge

CVFF: consistent valence force field

LAMMPS: large-scale atomic/molecular massively parallel simulator

G': storage moduli

G'': loss moduli

Abstract

Several *N*-[(2-Hydroxyl)-propyl-3-trimethyl ammonium] chitosan chlorides (HTCCs) with various degree of substitution (DS) were synthesized. The interaction of these compounds with sodium alginate(SA) in solutions and films was studied by rheology, Fourier transform infrared spectroscopy (FTIR), scanning electron microscopy (SEM), differential scanning calorimetry (DSC), and dynamic-mechanical analysis (DMA). The effects of some key factors such as DS, mass ratio of HTCC to SA ($m_{\mathrm{HTCC}}/m_{\mathrm{SA}}$), and temperature on the intermolecular interactions were investigated. The rheological results revealed the polyelectrolyte complex (PEC) solutions to be non-Newtonian fluids in all cases, showing a shear-thinning behavior. The apparent viscosity and viscoelastic properties of these HTCC compounds were observed to depend on DS and $m_{\mathrm{HTCC}}/m_{\mathrm{SA}}$. Thus, a high DS and low $m_{\mathrm{HTCC}}/m_{\mathrm{SA}}$ resulted in low apparent viscosities, which was ascribed to a shielding effect of N,N,N-trimethylammonium ($-N(CH_3)_3^+$) on the carboxyl ($-COO^-$) groups. Below the critical temperature (25 ºC), intermolecular interactions were dominated by hydrogen-bonds, while above this temperature electrostatic interactions prevailed. Both biomacromolecules showed maximum synergic effects and resulted in optimum HTCC/SA PEC structures for DS, $m_{\mathrm{HTCC}}/m_{\mathrm{SA}}$, and temperature of 96%, 1/10, and 25 °C, respectively. The properties of the HTCC-SA films confirmed a strong hydrogen-bonding and electrostatic interaction synergy between both biomacromolecules. The intermolecular interactions were elucidated by molecular dynamics studies. These results can provide a theoretical approach for synthetizing HTCC-SA based edible packaging films.

Keywords: *N*-[(2-Hydroxyl)-propyl-3-trimethyl ammonium] chitosan chloride, sodium alginate, synergistic effect, rheological properties, film properties

1 Introduction

Natural polymers including chitin/chitosan, sodium alginate, cellulose, starch, protein are ideal raw materials for composite biomaterials owing to their

biodegradability, biocompatibility, low toxicity and renewability. Polyelectrolyte complex (PEC) based biomaterials represent an innovative concept for coating and packaging production to be used in a wide range of food products (Costa-Almeida, Gasperini, Borges, Babo, Rodrigues, Mano, et al., 2017; Marciel, Chung, Brettmann, & Leon, 2017; Rodrigues, Oliveira, Costa, & Mano, 2016).

Sodium alginate (SA), extracted from sea weeds having (1,4)-linked β-D-mannuronate(M) and α-L-glucuronate (G) residues is widely used in the food packaging(Oliveira Filho, Rodrigues, Valadares, Almeida, Lima, Takeuchi, et al., 2019; Yao, Zhou, Chen, Ma, Li, & Chen, 2018), drug delivery(Agüero, Zaldivar-Silva, Peña, & Dias, 2017), textile(Li, He, & Huang, 2017), and cosmetic fields(Bae, Nam, & Park, 2019), among others. Owing to its polyanionic nature, SA can form PECs with positively charged polymers in the absence of organic solvents(Doi & Kokufuta, 2011; Paques, van der Linden, van Rijn, & Sagis, 2014). Based on these advantages, SA-based PECs are commonly used as bone tissue engineering scaffolds, drug packaging/controlled release agents, and functional food additive carriers(Mirpoor, Hosseini, & Yousefi, 2017; Xiao, Yu, & Yang, 2011; Zimet & Livney, 2009).

Among the numerous SA-based PECs, SA-chitosan PECs are typical examples of structures having superior flexibility and thermochemical/mechanical properties than their corresponding counterparts with pure SA and chitosan (Basim; & Deeb, 2013; Dominika Kulig, Anna Zimoch-Korzycka, Andrzej Jarmoluk, & Krzysztof Marycz, 2016). For instance, the strong interactions between SA and chitosan induced the formation of a SA-chitosan complex structure, which resulted in significant increases of the Young's modulus (by 280%) and the yield strength (by 219%) (Li, Ramay, Hauch, Xiao, & Zhang, 2005). Based on the intermolecular interactions, SA-chitosan hydrogels (Baysal, Aroguz, Adiguzel, & Baysal, 2013; Lv, Liu, Song, Tong, Shi, Zhao, et al., 2019), SA-chitosan biguanidine hydrochloride bioactive edible films (Salama, Aziz, & Sabaa, 2018), SA-chitosan porous membranes (Ma, Yu, & Ma, 2007), SA-chitosan nanoparticles (Liu, Xiao, Li, Shi, Li, & Huang, 2018; Motwani, Chopra, Sarmento, Ribeiro, Veiga, Sampaio, Neufeld, & Ferreira, 2007, Talegaonkar, Kohli, Ahmad, & Khar. 2008), and similar PECs have been prepared. The intermolecular interactions

including hydrogen bonding, electrostatic interaction, Van der Waals interaction provide SA-chitosan PECs with excellent properties. The properties of SA-chitosan PECs were dependent on the crosslinking density between SA and chitosan (Baysal, Aroguz, Adiguzel, & Baysal, 2013), the polymer ratio, the binding degree(Dominika, Anna, Andrzej, & Krzysztof, 2016), the net charge ratio, the molecular weights, and the preparation method of the samples (Sæther, Holme, Maurstad, Smidsrød, & Stokke, 2008). However, chitosan only dissolves in acidic solutions, which affects negatively to the functions and properties of the SA-chitosan PECs, limiting wide applications (Jiao, Niu, Ma, Li, Tay, & Chen, 2017). To overcome these drawbacks, hydrophilic modification of chitosan is required.

In our previous work, we reported the synthesis of water-soluble *N*-[(2-Hydroxyl)-propyl-3-trimethyl ammonium] chitosan chloride (HTCC) at different solvent pH values (Yang, Zhang, Qiao, Mu, Li, Xu, et al., 2015). HTCC is the best candidate for preparing HTCC-SA PECs. However, to our knowledge, there are no studies on HTCC-SA PECs at present, as well as the effect of HTCC in HTCC-SA PECs. To reveal the relationship between the intermolecular interactions and the PEC properties, the HTCC-SA PEC solutions were studied systematically by rheology. The HTCC-SA PEC films were also prepared and characterized by Fourier transform infrared spectroscopy (FTIR), scanning electron microscopy (SEM), differential scanning calorimetry (DSC), and dynamic-mechanical analysis (DMA). We believe that this research can provide information at the molecular level, providing a theoretical guideline for preparing HTCC/SA PECs for food packaging applications.

2 Experimental

2.1 Materials

We used the same chitosan (degree of deacetylation: 91.2%, determined by elemental analysis; viscosity: 200 mPa·s, provided by a vendor), 2,3-epoxypropyltrimethyl ammonium chloride (EPTAC), and HTCC as those in our previous work(Wang, Yang, Qiao, Li, Li, & Xu, 2018). HTCC with varying degree of substitution (DS, 50%, 83%, and 96%) were used herein. SA (food grade, viscosity: 60

mPa·s, M/G ratio of 1.5, provided by the vendor), was kindly supplied by the Qingdao Brightmoon Seaweed Group Co., Ltd.

2.2 Preparation of the HTCC-SA PECs solutions

Mother solutions of HTCC and SA with the same concentrations of 40 g/L were prepared. Typically, 8 g SA powder was added into a 200 mL beaker with 100 mL deionized water. To speed up the dissolution of SA, the beaker was sealed with preservative film, placed in a water bath at 60 ºC and electromagnetically stirred for 12 h. The mother solutions were then left settled down at room temperature for 24 h.

Before preparing the HTCC-SA PECs solutions, the mother solutions of HTCC and SA were heated to 60 ºC and electromagnetically stirred for 2 h, respectively. And then, a certain amount of HTCC and SA mother solutions, and deionized water were mixed and loaded in a series of 50.0 mL bottles with caps. To improve the formation of optimum HTCC-SA PEC structures, the corresponding sealed bottles were placed in a water bath at 60 ºC and electromagnetically stirred for another 4 h. The mixed solutions were left settled down at room temperature for 12 h.

The total weight was set up to 25.0 g, and the concentration of SA was fixed at 20 g/L in all cases. The $m_{\mathrm{HTCC}}/m_{\mathrm{SA}}$ used herein were 0/10 (pure SA), 1/10, 2/10, 4/10 and 10/0 (pure HTCC).

2.3 Preparation of the HTCC-SA PECs films

HTCC-SA PEC films were prepared by casting the as-prepared HTCC/SA solutions with various mass ratios in Teflon plates (inner diameter of 80 mm) and subsequent drying at 40 ºC for 24 h. A ventilated oven (DHG-9023A, Shanghai Yiheng Scientific Instrument Co., China) was used.

The as-obtained sample films were vacuum-dried at 80 °C for 60 min to obtain dry sample films. These dried films were conditioned at 25 °C in desiccators for at least two weeks at a relative humidity of 60 % for further analysis. The moisture contents of the films are indeed a critical parameter, which are determined by gravimetrically. The moisture contents are 22% (pure SA), 20% ($m_{\mathrm{HTCC}}/m_{\mathrm{SA}}$=1/10), 21% ($m_{\mathrm{HTCC}}/m_{\mathrm{SA}}$=4/10) and 15% (pure HTCC), respectively.

The thickness of the films was measured using an electronic digital Vernier caliper (Shenzhen Duliang Precision Machinery Co., Ltd.) with a sensitivity of 0.01 mm at 5 random positions for each film. The average thickness was 0.32 (pure SA), 0.17 (m_{HTCC} / m_{SA}=1/10), 0.15 (m_{HTCC} / m_{SA}=1/10) and 0.15 mm (pure HTCC), respectively.

2.4 Characterization of the HTCC-SA PECs

2.4.1 Rheological measurements

The rheological properties of the HTCC, SA, and HTCC-SA PEC solutions were studied on a DHR-2 rheometer (TA Instrument, USA) with a parallel plate geometry (45.0 mm in diameter and 1.0 mm in gap). Briefly, a fixed angular frequency (ω) of 1.0 rad/s was used to determine the linear viscoelastic region (i.e., the region in which the storage and loss moduli were independent of the strain). The storage modulus (G') and the loss modulus (G'') were measured within an angular frequency range of 0.1-100 rad/s at 25 ºC (unless special notification). When measuring the apparent viscosity, the shear rate was typically increased from 0.1 to 100 s^{-1} within 15 min.

The influence of the temperature, m_{HTCC}/m_{SA}, and the DS of HTCC on the rheological properties were investigated. The temperature was controlled with a Peltier temperature controller.

2.4.2 FTIR spectra

A Nicolet iS10 infrared spectrometer (Thermo Fisher Scientific Inc., Waltham, MA) with an attenuated total reflectance (ATR) accessory was used to obtain the FTIR spectra of the HTCC-SA PEC films. The samples were scanned from 4000 to 400 cm^{-1} 64 times and the resolution ratio was 4 cm^{-1}.

2.4.3 Morphologies

An EVO18 field-emission scanning electron microscope (Carl Zeiss, AG, Germany) provided with a field-emission source was used to characterize the cross-section morphologies of the PEC films. The microscope was operated at an accelerating voltage of 5.0 kV. The HTCC-SA PEC samples were freeze-dried and sputtered with gold before the observations.

2.4.4 DSC measurements

The DSC measurements were performed on a Q2000 TA instrument. All samples were heated from -50 to 175 ºC with a heating rate of 10 ºC/min. High purity nitrogen was used as the purge gas at a flow rate of 50 mL/min.

2.4.5 DMA

A DMA Q800 instrument (TA instruments, U.S.) was used to determine the dynamic mechanical properties of the HTCC-SA PEC films. The tests were carried out under the tensile mode from -50 to 160 ºC at 1.0 Hz and with a stain amplitude of 0.1%. The heating rate was 3.0 ºC/min. The dimensions of the PEC films were fixed at 20.0 × 10.0 mm. The glass-transition temperature (T_g) was obtained from the tanδ-temperature curve.

2.5 **Molecular simulations**

The size of the simulation box was 34.0 Å × 34.0 Å × 34.0 Å and periodic boundary conditions were employed in three dimensions. The model of the SA solution system consisted of 1000 water molecules and 10 SA repeated units. To study the effect of HTCC on the properties of the HTCC-SA PEC solution, a certain amount of HTCC repeat units with different DSs were added to the SA solutions. The Lennard-Jones (LJ) potential was used to describe the molecular interaction. A simple point charge (SPC) model was used to describe the water molecules, and the consistent valence force field (CVFF) and the corresponding atomic charges were used to describe the SA and HTCC molecules. The standard Lorentz-Berthelot mixing rules were used to calculate the LJ parameters between the different atoms. All electrostatic interactions were handled using the Ewald summation technique.

Molecular dynamic simulations were conducted on an NPT (T=298 K, P=1 atm) ensemble to simulate the dynamic process of the SA and HTCC/SA solution systems by using the large-scale atomic/molecular massively parallel simulator (LAMMPS) code. The entire simulation process was conducted for 80 ns. During the simulation process, the Nosé-Hoover thermostat and a barostat were chosen to keep the temperature and pressure constant. The damping constant of temperature and pressure was 0.1 ps.

3. Results and discussion

3.1 Effect of the HTCC DS on the rheological properties

At $m_{\mathrm{HTCC}}/m_{\mathrm{SA}}$: 1/10, c_{SA} : 20 g/L and 25 ºC, all the sample solutions showed a shear-thinning behavior(Fig.1a). The DS of HTCC in the pure solution was 50%, while those in HTCC-SA PEC solutions were 50, 83, and 96%. The apparent viscosities of the PEC and pure SA solution were all lower than that of the pure HTCC solution. The viscosity of the PEC solutions decreased with the DS of HTCC. According to our previous study(Wang, Qiao, Gao, Yang, Li, & Li, 2017), the high apparent viscosity of the pure HTCC solution can be attributed to the presence of stretched HTCC molecules as a result of electrostatic repulsion between $-\mathrm{N}(\mathrm{CH}_3)_3^+$ groups. The addition of small amounts of HTCC to the SA solution resulted in $-\mathrm{N}(\mathrm{CH}_3)_3^+$ groups replacing $-\mathrm{COO}^-$ groups, which favored intermolecular aggregation and decreased the apparent viscosity. At fixed $m_{\mathrm{HTCC}}/m_{\mathrm{SA}}$, the HTCC with DS of 50% possessed a limited number of $-\mathrm{N}(\mathrm{CH}_3)_3^+$ groups to replace $-\mathrm{COO}^-$ groups, resulting in minor intermolecular aggregation. Therefore, the apparent viscosity of HTCC (DS 50%)-SA PECs was only slightly lower than that of pure SA. Higher HTCC DS increased the number of $-\mathrm{N}(\mathrm{CH}_3)_3^+$ groups replacing $-\mathrm{COO}^-$ groups, promoting the formation of large amounts of aggregates with more ordered structures and resulting in a low apparent viscosity. This phenomenon indicated that the increasing of DS led to a good miscibility between HTCC and SA. These results were in the line with those reported by Yang et al. (Yang, Chen, & Fang, 2009) and Wyatt et al. (Wyatt, Gunther, & Liberatore, 2011). As revealed by Wyatt et al., the salt molecules generated repulsive interactions between the polymer chains, allowing close contact between chains and reducing viscosity.

The relationship between the apparent viscosity and the shear rates could be described by the Cross model (Wang, Qiao, Gao, Yang, Li, & Li, 2017; Wang, Yang, Qiao, Li, Li, & Xu, 2018). The fitted values of m for the HTCC-SA PECs were 0.35 (DS 50%), 0.38 (DS 83%) and 0.36 (DS 96%). These values were lower than those of the pure HTCC (0.79 at DS 50%) (Wang, Qiao, Gao, Yang, Li, & Li, 2017), SA

(0.65)(Ma, Lin, Chen, Zhao, & Zhang, 2014) and HTCC-CMC systems (0.41)(Wang, Yang, Qiao, Li, Li, & Xu, 2018). As reported elsewhere(Le Goff, Gaillard, Helbert, Garnier, & Aubry, 2015), low *m* values are indicative of shear-thinning behavior and weak gel properties for the HTCC-SA PEC solutions.

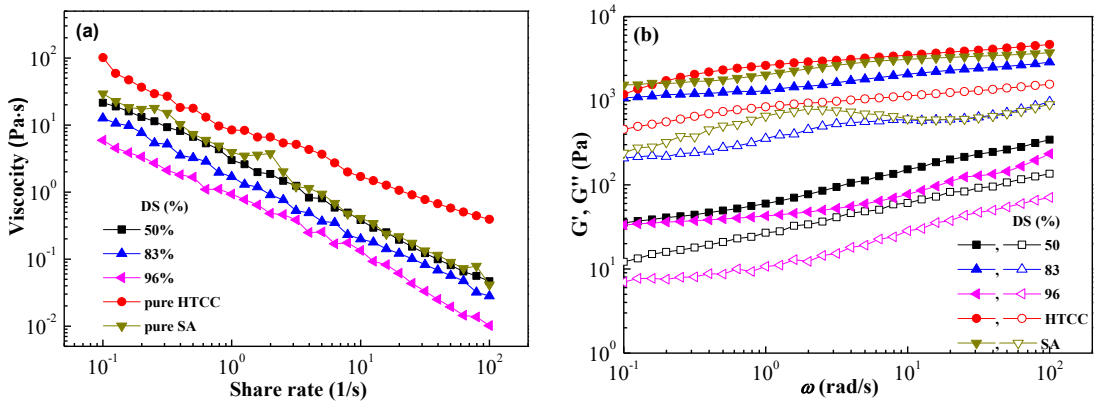

Fig.1 (a) Viscosity *vs*. shear rate and (b) storage (G', filled symbols) and loss (G'', open symbols) moduli *vs*. ω for HTCC and HTCC-SA PEC solutions at 25 ºC.

Fig.1b shows the viscoelastic properties of HTCC-SA PECs with different HTCC DS values. In all cases, the storage moduli (G') were significantly higher than the loss moduli (G''), and both values were slightly dependent on ω. These results indicated that the HTCC-SA PEC solutions showed high elasticity and were comprised by gel-like structures (Dai, Zhan, Wei, Sun, Mao, McClements, et al., 2018). The low G''/G' ratios (Table 1) confirmed the high elasticity of the solutions(Le Goff, Gaillard, Helbert, Garnier, & Aubry, 2015). The G' of pure HTCC was slightly higher than that of pure SA, followed by those of HTCC(DS 83%)/SA, HTCC(DS 50%)/SA, and HTCC(DS 96%)/SA PEC solutions. These results were consistent with the apparent viscosities obtained. Thus, $-N(CH_3)_3^+$ groups shielded $-COO^-$ groups, favoring the formation of HTCC-SA intermolecular aggregations, which were prominently elastic at the frequency investigated herein(Lozano-Vazquez, Lobato-Calleros, Escalona-Buendia, Chavez, Alvarez-Ramirez, & Vernon-Carter, 2015).

Table 1 G''/G' ratios for HTCC-SA PECs with different HTCC DSs at four angular frequencies.

HTCC DS	G''/G' ±			
(%)	0.1 rad/s	1 rad/s	10 rad/s	100 rad/s
50	0.34±0.004	0.45±0.005	0.40±0.005	0.39±0.006

83	0.19±0.002	0.27±0.003	0.28±0.005	0.34±0.004
96	0.21±0.004	0.25±0.004	0.37±0.005	0.30±0.003
96[a]	0.38±0.006	0.32±0.003	0.33±0.004	0.33±0.003
SA	0.16±0.002	0.32±0.005	0.20±0.004	0.24±0.004

[a]- pure HTCC solution(Wang, Qiao, Gao, Yang, Li, & Li, 2017).

3.2 Effect of $m_{\mathrm{HTCC}}/m_{\mathrm{SA}}$ on the rheological properties

The variation of the apparent viscosity of HTCC-SA PECs (DS: 96%) with $m_{\mathrm{HTCC}}/m_{\mathrm{SA}}$ (1/10, 2/10 and 4/10) for several shear rates is depicted in Fig.2a. The apparent viscosity of the HTCC-SA PEC solution with $m_{\mathrm{HTCC}}/m_{\mathrm{SA}}$ =1/10 was significantly lower than those of other two PEC solutions ($m_{\mathrm{HTCC}}/m_{\mathrm{SA}}$ =2/10 and 4/10). According to supplier, the viscosity of HTCC (200 mPa·s) is ca. 3 times higher than that of SA (60 mPa·s). Therefore, for a $m_{\mathrm{HTCC}}/m_{\mathrm{SA}}$ of 1/10, the number of $-\mathrm{N}(\mathrm{CH}_3)_3^+$ groups is relatively low to shield the $-\mathrm{COO}^-$ groups. This favored HTCC-SA intermolecular aggregation and the apparent viscosity of the HTCC-SA PECs decreased as a result. A further increase of $m_{\mathrm{HTCC}}/m_{\mathrm{SA}}$ favored the onset of strong electrostatic interactions between $-\mathrm{N}(\mathrm{CH}_3)_3^+$ and $-\mathrm{COO}^-$, inducing the formation of large HTCC-SA PEC aggregates and therefore increasing the apparent viscosity of the solution. These results were similar to those reported by Goycoolea et al. (Goycoolea, Lollo, Remuñán-López, Quaglia, & Alonso, 2009), Qiao et al.(Qiao, Ma, Zhang, & Yao, 2017), and Chiappisi et al.(Chiappisi, Hoffmann, & Gradzielski, 2013).

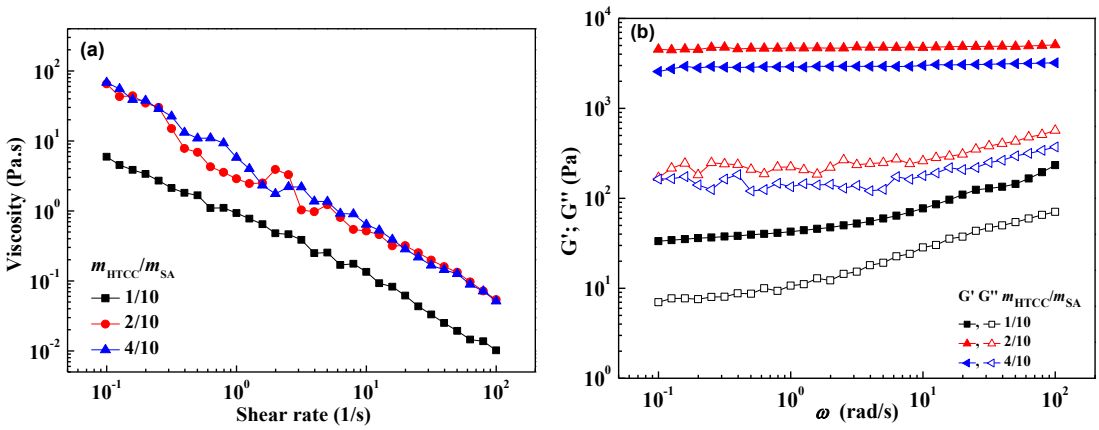

Fig.2 (a) Viscosity *vs.* shear rate, and (b) storage (G', solid symbols) and loss (G'', empty symbols) moduli *vs.* ω for HTCC/SA with different mass ratios at 25 ºC.

The elasticity of the HTCC-SA PEC solutions for different $m_{\mathrm{HTCC}}/m_{\mathrm{SA}}$ ratios (Fig.2b) revealed the presence of a gel-like structure(Jia, Chen, Shi, Ye, Abid, Jabbar, et al., 2014). The HTCC (1/10)-SA solution showed the lowest G', while the HTCC(2/10)-SA PEC solution showed the highest G' value. In the case of HTCC/SA(1/10), the low G' value could be ascribed to: (i) the aggregation of SA induced by the shielding effect of $-\mathrm{N}(\mathrm{CH}_3)_3^+$ on $-\mathrm{COO}^-$ groups and (ii) the presence of hydrophobic interactions. Increasing $m_{\mathrm{HTCC}}/m_{\mathrm{SA}}$ resulted in a higher number of joint points, which facilitated the formation of HTCC-SA interpenetrating networks via electrostatic interaction between $-\mathrm{N}(\mathrm{CH}_3)_3^+$ and $-\mathrm{COO}^-$ groups, due to a good miscibility between the two biomacromolecules. Therefore, the HTCC-SA(2/10, 4/10) PEC solutions showed much higher G' values than the HTCC-SA(1/10) PEC solution, and 2/10 was selected as the $m_{\mathrm{HTCC}}/m_{\mathrm{SA}}$ optimum ratio. For the HTCC-SA(2/10 and 4/10) PEC solutions, the independence of G' on ω confirmed the formation of gel structures.

3.3 Effect of the temperature on the rheological properties

At a fixed $m_{\mathrm{HTCC}}/m_{\mathrm{SA}}$ (1/10, DS: 96%), the viscosity decreased slightly with temperature for the 15-25 ºC range, and this increase was significantly higher for

temperatures up to 35 ºC (Figs.3a and b). The viscoelasticity of the PEC solutions (Figs.3c and d) showed a similar trend with temperature. On one hand, increasing the temperature weakened hydrogen-bonding, favoring electrostatic and hydrophobic interactions(Koussathana, Lianos, & Staikos, 1997) and increasing the viscosity. On the other hand, higher temperatures promote molecular movement, which decreases the electrostatic interaction and the viscosity(García-Ochoa, Santos, Casas, & Gómez, 2000; Lu & Weiss, 1992). This trend revealed that hydrogen-bonding was mostly responsible for viscosity over the 15-25 ºC range, electrostatic interaction prevailed over the range 25-35 ºC. The result was consistent with those obtained by Razavi et al. (Razavi, Alghooneh, & Behrouzian, 2018) and Moreira et al.(Moreira, Chenlo, Silva, & Torres, 2017). Thus, 25 ºC might be the critical temperature at which the viscosity reached a critical value.

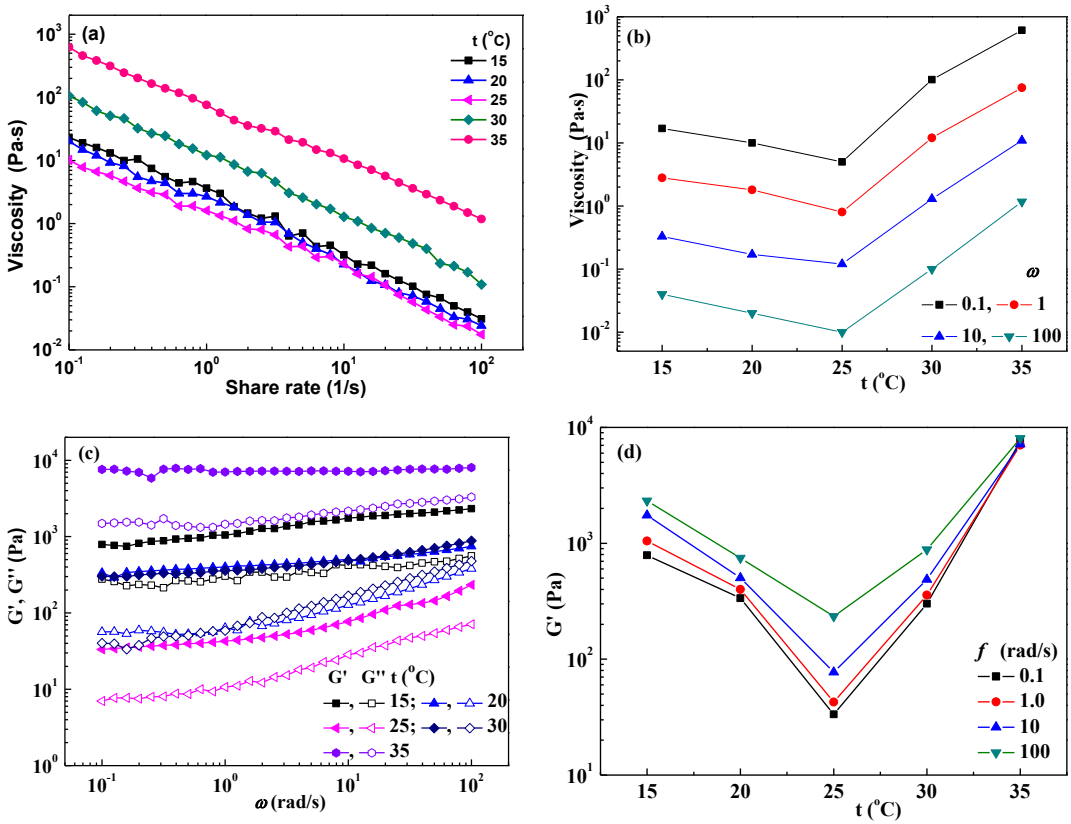

Fig.3 Apparent viscosity *vs*. shear rate (a), temperature (b) at different shear rates, and (c) storage (G', filled symbols) and loss (G'', open symbols) moduli *vs*. ω for HTCC-SA (m_{HTCC} / m_{SA}=10%) PECs at (d) 15, 20, 25, 30 and 35 ºC.

3.4 FTIR analysis

To investigate the interaction between the HTCC and SA molecules, pure HTCC, SA, and HTCC-SA (m_{HTCC} / m_{SA} =40% as an example) PEC films were prepared and characterized by ATR-FTIR spectroscopy (Fig. 4). HTCC showed typical adsorption peaks at 3352 (ν_s(-OH) and ν_s(-NH)), 3258 (ν_s(-CH)) (Tan, Zhang, Luan, Wei, Chen, Dong, Li, & Guo, 2017), 2919 (ν_s(-CH_3), ν_{as}(-CH_2)), 2849 (ν_s(-CH_2) (Hu, Wang, & Wang, 2016), at 1648 (ν_s(N-H) of HN-C=O), 1573(ν_{as}(C=O) and ν_{as}(O-H) of bound water), 1475 (δ(-CH) in $N(CH_3)_3^+$)(Yang, et al., 2015). For SA, the characteristic peaks appeared at 1592 (ν_{as}(C=O)), 1405 (ν_s(C=O)) and 1124 (ν_s(C-C))(Liu, Li, & Li, 2017). These characteristic peaks were also observed in HTCC-SA PEC films, and some of them were red-shifted. For example, the adsorption peak at 3352 cm^{-1} (ν_s(-OH)) were red-shifted to 3245 cm^{-1}, and this was ascribed to the formation of hydrogen bonds between the two biomacromolecules(Wang, Yang, Qiao, Li, Li, & Xu, 2018). The absorption peak at 1475 cm^{-1} (δ(CH) in $N(CH_3)_3^+$) was red-shifted to 1469 cm^{-1} as a result of the electrostatic interaction between the $-N(CH_3)_3^+$ and $-COO^-$ groups(Silva-Weiss, Bifani, Ihl, Sobral, & Gómez-Guillén, 2013). These red-shifting suggested that the HTCC-SA PECs were formed by electrostatic interaction or hydrogen bonds between the two oppositely charged biomacromolecules (Baysal, Aroguz, Adiguzel, & Baysal, 2013).

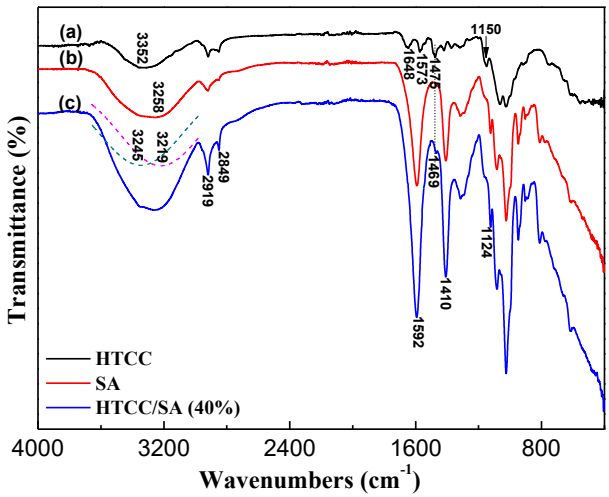

Fig.4 FTIR spectra of HTCC (a), SA (b) and HTCC-SA(4/10) films.

3.5 Molecular simulation results

Molecular simulations revealed the formation of HTCC-SA aggregates with more ordered structures compared to pure SA. This was ascribed to electrostatic and hydrogen bond interactions between HTCC and the SA molecules, as shown in Fig.5. At a fixed m_{HTCC}/m_{SA}, the joint points between HTCC and the SA molecules increased with HTCC DS, promoting the formation of more ordered HTCC-SA aggregate structures (Fig.5a). Larger HTCC-SA PEC aggregates were formed as m_{HTCC}/m_{SA} increased (Fig.5b). These results were consistent with the apparent viscosities (Figs.1 and 2). Thus, the apparent viscosity decreased upon increasing HTCC DS, and increased with m_{HTCC}/m_{SA}.

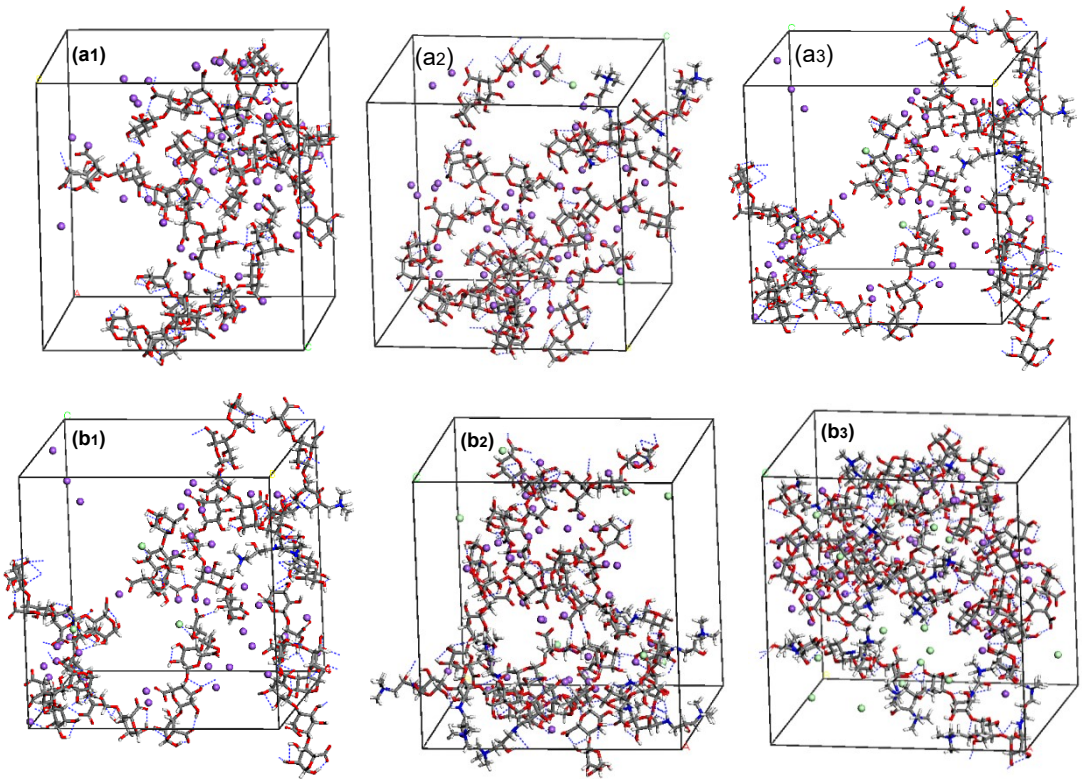

Fig. 5 (a) Equilibrium configurations of pure SA(a1), HTCC(50%)-SA(a2) and HTCC(100%)-SA (a3) samples, and (b) those of HTCC-SA PECs with m_{HTCC}/m_{SA} of 1/10(b1), 2/10(b2) and 4/10(b3), respectively. Red, white, gray, blue, violet and green dots correspond to O, H, C, N, Na^+ and Cl^- atoms (or ions), respectively. The blue dot lines represent hydrogen bonds.

3.6 SEM observations

Cross-section SEM images of HTCC, SA and HTCC-SA PEC films with various

m_{HTCC} / m_{SA} ratios are shown in Fig.6. The addition of THCC to the SA films having m_{HTCC} / m_{SA} of 1/10, 2/10, and 4/10 produced different fractures of the films. Thus, the pure SA film showed a clear three-dimensional network structure which was mainly ascribed to the intermolecular hydrogen bond interactions. At a m_{HTCC} / m_{SA} of 1/10, compacted aggregates were observed by the shielding effect of the $-N(CH_3)_3^+$ groups over the $-COO^-$ groups, which resulted in the aggregation of HTCC and SA biomacromolecules(Kulig, Zimoch-Korzycka, Jarmoluk, & Marycz, 2016). When the m_{HTCC} / m_{SA} ratio increased to 2/10 and 4/10, the electrostatic interaction between the $-N(CH_3)_3^+$ groups of the linear HTCC molecules and the $-COO^-$ groups of SA molecules stretched the SA chains in the PEC film. This stretching of the SA structure increased with the m_{HTCC} / m_{SA} ratio and a laminar structure appeared at a m_{HTCC} / m_{SA} of 4/10. The variation of the HTCC/SA fracture upon increasing m_{HTCC} / m_{SA} confirmed the presence of strong intermolecular interactions between the HTCC and SA molecules, as revealed by the rheological studies, (Figs.1, 2, and 4). The intermolecular interactions are schematically illustrated in Figs.1b and 2b.

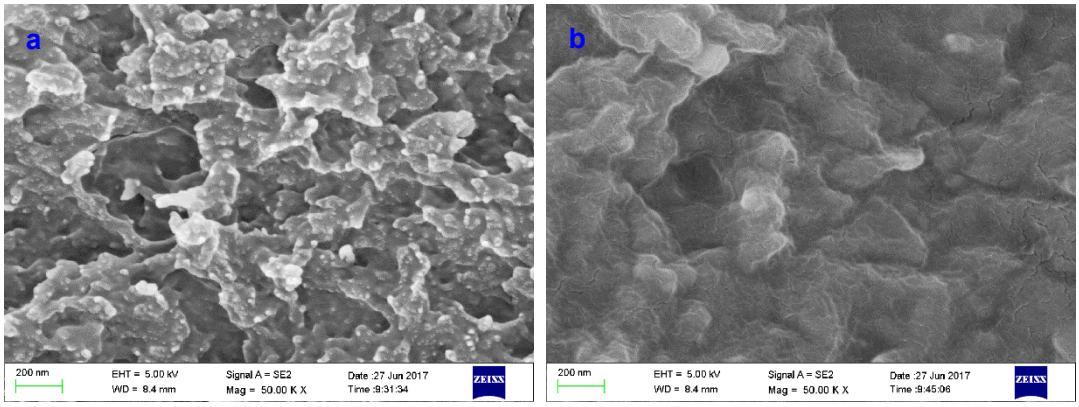

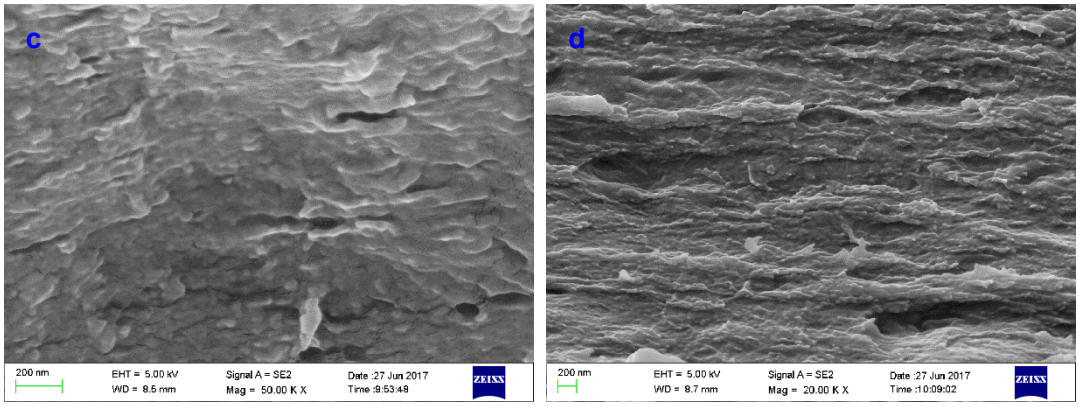

Fig.6 Cross-section SEM images of HTCC/SA films with mass ratios of 0%(a), 10%(b), 20%(c), and 40%(d). The DS of HTCC was 0.96.

3.7 Thermal properties

The thermal properties of the PEC films were characterized by DSC(Fig.7). The large amount of -OH, -COO^-, and -NH groups in the HTCC and SA molecules favor the adsorption of water, which was released with temperature. The broad endothermic peak at 106-120 ºC was attributed to the loss of bonded water. The enthalpy of this peak has been reported to correspond with content of bonded water, while the temperature of the peak is related to the structure of the networks (Wang, Yang, Qiao, Li, Li, & Xu, 2018). The HTCC/SA(1/10) film showed higher bonded water vaporization temperature (*t*) than pure SA, but lower than HTCC (96%) (Table 2). According to the results of rheology, SEM, and simulation, at a $m_{\mathrm{HTCC}}/m_{\mathrm{SA}}$ of 1/10, the low amounts of $-\mathrm{N(CH_3)_3^+}$ hardly shielded the relatively surplus of $-\mathrm{COO^-}$ groups in SA, inducing the aggregation of SA molecules. Thus, the bonded water was encapsulated in these networks and the three-dimensional structure hindered heat transfer, which resulted in higher bonded water vaporization temperatures. When the $m_{\mathrm{HTCC}}/m_{\mathrm{SA}}$ increased to 2/10, the SA molecules stretched and the thermal conductivity increased, which resulted in lower *t*. As $m_{\mathrm{HTCC}}/m_{\mathrm{SA}}$ further increased to 4/10, the HTCC and SA chains in the PEC film were more closely by strong electrostatic interactions(Kulig, Zimoch-Korzycka, Jarmoluk, & Marycz, 2016), the bonded water was encapsulated in the network tightly, and this resulted in maximum *t* values. The enthalpy changes (i.e. the endothermic peak areas) revealed that the HTCC-PEC (4/10) PEC bonded a higher

amount of water compared to the HTCC-PEC (1/10 and 2/10) PECs, which is consistent with the simulated results. The volume of HTCC-SA (4/10) PEC was much larger than those of the HTCC-SA (1/10 and 2/10) PECs. The high *t* and large ΔH observed for pure SA and HTCC were ascribed to the steric-hindrance and the presence of large amounts of -OH, -COO$^-$, and -NH groups.

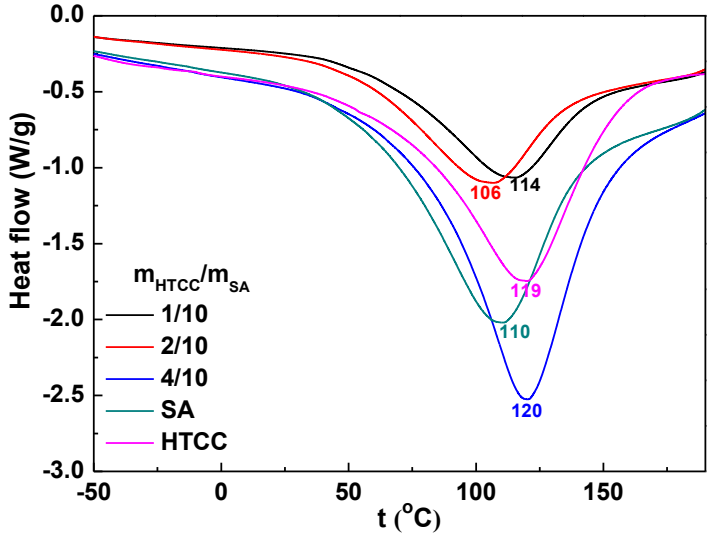

Fig.7 DSC spectra of the HTCC-SA PEC films with different mass ratios.

Table 2 Bonded water vaporization temperature (t) and enthalpy (ΔH) for the HTCC-SA PEC films with different mass ratios.

Samples	SA	1/10	2/10	4/10	HTCC
t (°C)	110	114	106	120	119
ΔH (J/g)	295	219	222	323	302

3.8 DMA

DMA is highly sensitive to changes of internal molecular mobility and can be used to determine the phase structure and morphology of polymers. HTCC showed a broad peak at ca. 60 °C upon increasing temperature (Fig.8a). According to our previous study(Yang, et al., 2015), this peak can be ascribed to *α* relaxation, which is controlled by partial motion of molecular segments. The temperature was defined as T_g. The T_g of SA, and the HTCC-SA PEC films was 44, 65 (m_{HTCC}/m_{SA}=1/10) and 65 (m_{HTCC}/m_{SA} =4/10) °C, respectively. The T_g of the HTCC-SA PEC films showed a positive deviation

from the linear mixing rule, revealing the miscibility of two molecules via strong intermolecular interactions, the formation of a PEC structure, and the restriction of the chain movement(Lu & Weiss, 1992; Xu, Kuo, Lee, & Chang, 2002).

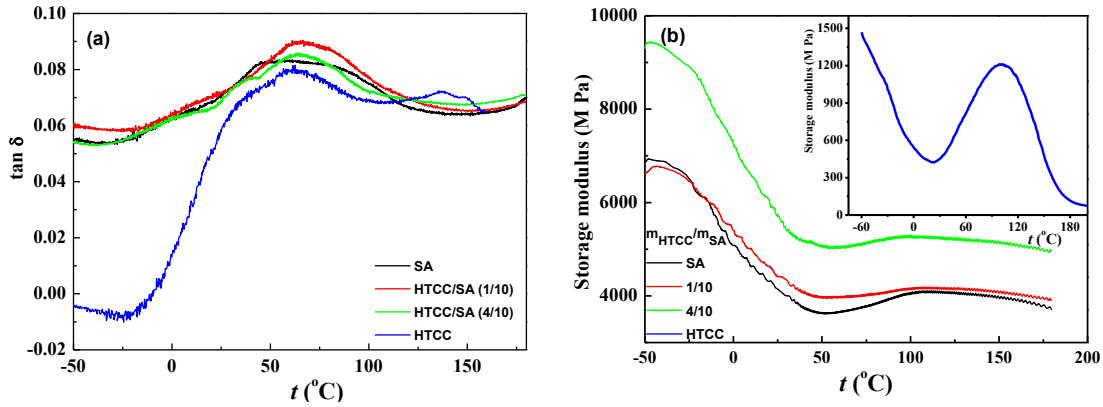

Fig.8 Temperature dependence of tanδ (a) and storage modulus (b) 1.0 Hz for the HTCC, SA, and HTCC/SA composite films with mass ratios of 1/10 and 1/40.

The storage modulus *vs*. temperature curves (Fig.8b) revealed the same variation of T_g with m_{HTCC}/m_{SA}. The storage moduli of pure SA (ca. 6800 MPa) and the HTCC-SA PEC films (ca. 6800 MPa-9400 MPa) were much higher than that of the pure HTCC film (ca. 1500 MPa). The storage modulus of the HTCC-SA(4/10) PEC film was significantly higher than that of the HTCC-SA(1/10) PEC films. Combined with the SEM results (Fig.6), these data could be ascribed to strong intermolecular electrostatic interactions between the HTCC and SA molecules. These strong interactions resulted in a stretched SA conformation and the formation of HTCC/CMC lamellar structures for a m_{HTCC}/m_{SA} of 4/10.

4. Conclusions

Hydrogen-bonding and electrostatic interactions were detected between the HTCC and SA molecules in both aqueous solution and films. At low m_{HTCC}/m_{SA} (e.g., 1/10) or DS of HTCC (e.g., 50%), the $-(CH_3)_3^+$ groups shielded the $-COO^-$ groups of SA, and hydrogen-bonding and hydrophobic interactions induced the aggregation of the HTCC-SA PECs. As a result, the apparent viscosity of the HTCC-SA PECs decreased and the viscoelasticity increased. In contrast, at high m_{HTCC}/m_{SA} or DS of HTCC values, the intermolecular electrostatic interaction between the $-(CH_3)_3^+$ and the

-COO^- groups induced the formation of entanglements, which determined the rheological properties of HTCC-SA PEC solutions. These entanglements formed by intermolecular electrostatic interaction were more stable than those formed through hydrophobic interactions, resulting in higher apparent viscosities and viscoelasticity. The synergetic effect of hydrogen-bonding and the electrostatic interaction depended on the temperature. Thus, below 25 ºC, hydrogen-bonding dominated the intermolecular interaction, while above 25 ºC electrostatic interaction prevailed. Hydrogen-bonding and electrostatic interactions resulted in the typical absorption peaks (3245, 3219 and 1469 cm^{-1}) to red-shift, while the HTCC-SA PEC steric structures shifted to lamellar ones, which increased the thermal stability.

Acknowledgments

The authors acknowledge the financial support from National Natural Science Foundation of China (21306092 and 21376125), and Program for Scientific Research Innovation Team in Colleges and Universities of Shandong Province.

Conflicts of Interest: The authors declare no conflict of interest.

References

Agüero, L., Zaldivar-Silva, D., Peña, L. & Dias, M.L. (2017). Alginate microparticles as oral colon drug delivery device: A review. *Carbohydrate Polymers, 168,* 32-43.

Bae, S.B., Nam, H.C. & Park, W.H. (2019). Electrospraying of environmentally sustainable alginate microbeads for cosmetic additives. *International Journal of Biological Macromolecules, 133,* 278-283.

Basim, A.-J., & Deeb, A.F. (2013). Modification the Rheological Behavior of Sodium Alginate by Chitosan and Multivalent electrolytes. *Italian Journal of Food Science, 25*, 196-201.

Baysal, K., Aroguz, A. Z., Adiguzel, Z., & Baysal, B. M. (2013). Chitosan/alginate crosslinked hydrogels: Preparation, characterization and application for cell growth purposes. *Int J Biol Macromol, 59*, 342-348.

Chiappisi, L., Hoffmann, I., & Gradzielski, M. (2013). Complexes of oppositely charged polyelectrolytes and surfactants – recent developments in the field of biologically derived polyelectrolytes. *Soft Matter, 9*(15), 3896-3909.

Costa-Almeida, R., Gasperini, L., Borges, J., Babo, P. S., Rodrigues, M. T., Mano, J. F., Reis, R. L., & Gomes, M. E. (2017). Microengineered Multicomponent Hydrogel Fibers: Combining Polyelectrolyte Complexation and Microfluidics. *ACS Biomaterials Science & Engineering, 3*(7), 1322-1331.

Dai, L., Zhan, X., Wei, Y., Sun, C., Mao, L., McClements, D. J., & Gao, Y. (2018). Composite zein - propylene glycol alginate particles prepared using solvent evaporation: Characterization and application as Pickering emulsion stabilizers. *Food Hydrocolloids, 85*, 281-290.

Doi, R., & Kokufuta, E. (2011). Conductometric and Light Scattering Studies on the Complexation between Cationic Polyelectrolyte Nanogel and Anionic Polyion. *Langmuir, 27*(1), 392-398.

Dominika, K., Anna, Z.-K., Andrzej, J., & Krzysztof, M. (2016). Study on Alginate-Chitosan Complex Formed with Different Polymers Ratio. *Polymers, 8*, 167-284.

García-Ochoa, F., Santos, V. E., Casas, J. A., & Gómez, E. (2000). Xanthan gum: production, recovery, and properties. *Biotechnology Advances, 18*(7), 549-579.

Goycoolea, F. M., Lollo, G., Remuñán-López, C., Quaglia, F., & Alonso, M. J. (2009). Chitosan-Alginate Blended Nanoparticles as Carriers for the Transmucosal Delivery of Macromolecules. *Biomacromolecules, 10*(7), 1736-1743.

Hu, D., Wang, H., & Wang, L. (2016). Physical properties and antibacterial activity of quaternized chitosan/carboxymethyl cellulose blend films. *LWT - Food Science and Technology, 65*, 398-405.

Jia, X., Chen, Y., Shi, C., Ye, Y., Abid, M., Jabbar, S., Wang, P., Zeng, X., & Wu, T. (2014). Rheological properties of an amorphous cellulose suspension. *Food Hydrocolloids, 39*, 27-33.

Jiao, Y., Niu, L.-n., Ma, S., Li, J., Tay, F. R., & Chen, J.-h. (2017). Quaternary ammonium-based biomedical materials: State-of-the-art, toxicological aspects and antimicrobial resistance. *Progress in Polymer Science, 71*, 53-90.

Koussathana, M., Lianos, P., & Staikos, G. (1997). Investigation of Hydrophobic Interactions in Dilute Aqueous Solutions of Hydrogen-Bonding Interpolymer Complexes by Steady-State and Time-Resolved Fluorescence Measurements. *Macromolecules, 30*(25), 7798-7802.

Kulig, D., Zimoch-Korzycka, A., Jarmoluk, A., & Marycz, K. (2016). Study on Alginate–Chitosan Complex Formed with Different Polymers Ratio. *Polymers, 8*(5), 167.

Le Goff, K. J., Gaillard, C., Helbert, W., Garnier, C., & Aubry, T. (2015). Rheological study of reinforcement of agarose hydrogels by cellulose nanowhiskers. *Carbohydrate Polymers, 116*, 117-123.

Li, J., He, J., & Huang, Y. (2017). Role of alginate in antibacterial finishing of textiles. *International Journal of Biological Macromolecules, 94,* 466-473.

Li, Z., Ramay, H. R., Hauch, K. D., Xiao, D., & Zhang, M. (2005). Chitosan–alginate hybrid scaffolds for bone tissue engineering. *Biomaterials, 26*(18), 3919-3928.

Liu, J., Xiao, J., Li, F., Shi, Y., Li, D., & Huang, Q. (2018). Chitosan-sodium alginate nanoparticle as a delivery system for ε-polylysine: Preparation, characterization and antimicrobial activity. *Food Control*, 91, 302-310.

Liu, S., Li, Y., & Li, L. (2017). Enhanced stability and mechanical strength of sodium alginate composite films. *Carbohydrate Polymers, 160*, 62-70.

Lozano-Vazquez, G., Lobato-Calleros, C., Escalona-Buendia, H., Chavez, G., Alvarez-Ramirez, J.,

& Vernon-Carter, E. J. (2015). Effect of the weight ratio of alginate-modified tapioca starch on the physicochemical properties and release kinetics of chlorogenic acid containing beads. *Food Hydrocolloids, 48*, 301-311.

Lu, X., & Weiss, R. A. (1992). Relationship between the glass transition temperature and the interaction parameter of miscible binary polymer blends. *Macromolecules, 25*(12), 3242-3246.

Lv, X., Liu, Y., Song, S., Tong, C., Shi, X., Zhao, Y., Zhang, J., & Hou, M. (2019). Influence of chitosan oligosaccharide on the gelling and wound healing properties of injectable hydrogels based on carboxymethyl chitosan/alginate polyelectrolyte complexes. *Carbohydrate Polymers, 205*, 312-321.

Ma, L., Yu, W., & Ma, X. (2007). Preparation and characterization of novel sodium alginate/chitosan two ply composite membranes. *Journal of Applied Polymer Science*, 106, 394-399.

Ma, J., Lin, Y., Chen, X., Zhao, B., & Zhang, J. (2014). Flow behavior, thixotropy and dynamical viscoelasticity of sodium alginate aqueous solutions. *Food Hydrocolloids, 38*, 119-128.

Marciel, A. B., Chung, E. J., Brettmann, B. K., & Leon, L. (2017). Bulk and nanoscale polypeptide based polyelectrolyte complexes. *Advances in Colloid and Interface Science, 239*, 187-198.

Mirpoor, S. F., Hosseini, S. M. H., & Yousefi, G. H. (2017). Mixed biopolymer nanocomplexes conferred physicochemical stability and sustained release behavior to introduced curcumin. *Food Hydrocolloids, 71*, 216-224.

Moreira, R., Chenlo, F., Silva, C., & Torres, M. D. (2017). Rheological behaviour of aqueous methylcellulose systems: Effect of concentration, temperature and presence of tragacanth. *LWT, 84*, 764-770.

Motwani, S.K., Chopra, S., Talegaonkar, S., Kohli, K., Ahmad, F.J., & Khar, R.K. (2008). Chitosan-sodium alginate nanoparticles as submicroscopic reservoirs for ocular delivery: Formulation, optimisation and in vitro characterisation. *European Journal of Pharmaceutics and Biopharmaceutics*, *68*, 513-525.

Oliveira Filho, J.G, Rodrigues, J.M., Valadares, A.C.F., Almeida, A.B., Lima, T.M., Takeuchi, K.P., Alves, C.C.F., Figueiredo Sousa, H.A., Silva, E.R., Dyszy, F.H. & Egea, M.B. (2019). Active food packaging: Alginate films with cottonseed protein hydrolysates. *Food Hydrocolloids*, *92*, 267-275.

Paques, J. P., van der Linden, E., van Rijn, C. J. M., & Sagis, L. M. C. (2014). Preparation methods of alginate nanoparticles. *Advances in Colloid and Interface Science, 209*, 163-171.

Qiao, C., Ma, X., Zhang, J., & Yao, J. (2017). Molecular interactions in gelatin/chitosan composite films. *Food Chemistry, 235*, 45-50.

Razavi, S. M. A., Alghooneh, A., & Behrouzian, F. (2018). Influence of temperature on sage seed gum (Salvia macrosiphon) rheology in dilute and concentrated regimes. *Journal of Dispersion Science and Technology, 39*(7), 982-995.

Rodrigues, M. N., Oliveira, M. B., Costa, R. R., & Mano, J. F. (2016). Chitosan/Chondroitin Sulfate Membranes Produced by Polyelectrolyte Complexation for Cartilage Engineering.

Biomacromolecules, 17(6), 2178-2188.

Sæther, H. V., Holme, H. K., Maurstad, G., Smidsrød, O., & Stokke, B. T. (2008). Polyelectrolyte complex formation using alginate and chitosan. *Carbohydrate Polymers, 74*(4), 813-821.

Salama, H.E., Aziz, M.S.A., & Sabaa, M.W. (2018). Novel biodegradable and antibacterial edible films based on alginate and chitosan biguanidine hydrochloride. *International Journal of Biological Macromolecules*, 116, 443-450.

Sarmento, B., Ribeiro, A., Veiga, F., Sampaio, P., Neufeld, R., & Ferreira, D. (2007). Alginate/Chitosan Nanoparticles are Effective for Oral Insulin Delivery. *Pharmaceutical Research, 24*(12), 2198-2206.

Silva-Weiss, A., Bifani, V., Ihl, M., Sobral, P. J. A., & Gómez-Guillén, M. C. (2013). Structural properties of films and rheology of film-forming solutions based on chitosan and chitosan-starch blend enriched with murta leaf extract. *Food Hydrocolloids, 31*(2), 458-466.

Tan, W., Zhang, J., Luan, F., Wei, L., Chen, Y., Dong, F., Li, Q., & Guo, Z. (2017). Design, synthesis of novel chitosan derivatives bearing quaternary phosphonium salts and evaluation of antifungal activity. *International Journal of Biological Macromolecules*, 102, 704-711.

Wang, A. (2008). *Chitin Chemistry*. Beijing: Chemical Industry Press.

Wang, B., Qiao, C., Gao, X., Yang, X., Li, Y., & Li, T. (2017). Rheological properties of N-[(2-hydroxyl)-propyl-3-trimethyl ammonium] chitosan chloride. *Carbohydrate Polymers, 171*(Supplement C), 50-58.

Wang, B., Yang, X., Qiao, C., Li, Y., Li, T., & Xu, C. (2018). Effects of chitosan quaternary ammonium salt on the physicochemical properties of sodium carboxymethyl cellulose-based films. *Carbohydrate Polymers, 184*, 37-46.

Wyatt, N. B., Gunther, C. M., & Liberatore, M. W. (2011). Increasing viscosity in entangled polyelectrolyte solutions by the addition of salt. *Polymer, 52*(11), 2437-2444.

Xiao, J., Yu, H., & Yang, J. (2011). Microencapsulation of sweet orange oil by complex coacervation with soybean protein isolate/gum Arabic. *Food Chemistry, 125*(4), 1267-1272.

Xu, H., Kuo, S.-W., Lee, J.-S., & Chang, F.-C. (2002). Glass transition temperatures of poly(hydroxystyrene-co-vinylpyrrolidone-co-isobutylstyryl polyhedral oligosilsesquioxanes). *Polymer, 43*(19), 5117-5124.

Yang, J., Chen, S., & Fang, Y. (2009). Viscosity study of interactions between sodium alginate and CTAB in dilute solutions at different pH values. *Carbohydrate Polymers, 75*(2), 333-337.

Yang, X., Zhang, C., Qiao, C., Mu, X., Li, T., Xu, J., Shi, L., & Zhang, D. (2015). A simple and convenient method to synthesize N-[(2-hydroxyl)-propyl-3-trimethylammonium] chitosan chloride in an ionic liquid. *Carbohydrate Polymers, 130*, 325-332.

Yao, J., Zhou, Y., Chen, X., Ma, F., Li, P., & Chen, C. (2018). Effect of sodium alginate with three molecular weight forms on the water holding capacity of chicken breast myosin gel. *Food Chemistry*, 239, 1134-1142.

Zimet, P., & Livney, Y. D. (2009). Beta-lactoglobulin and its nanocomplexes with pectin as vehicles for ω-3 polyunsaturated fatty acids. *Food Hydrocolloids, 23*(4), 1120-1126.